BIOCHEMISTRY
including biophysical chemistry & molecular biology
Article

Biochemistry **2010,** *49,* 5143–5153 5143
DOI: 10.1021/bi100563z

Structural Basis of the Recognition of the SAMP Motif of Adenomatous Polyposis Coli by the Src-Homology 3 Domain[†,‡]

Shuji Kaieda,[§] Chiyuki Matsui,[∥] Yuko Mimori-Kiyosue,[⊥] and Takahisa Ikegami*[,§]

[§]*Institute for Protein Research, Osaka University, 3-2 Yamadaoka, Suita, Osaka 565-0871, Japan,* [∥]*KAN Research Institute, Inc., 6-7-3 Minatojima-minamimachi, Chuo-ku, Kobe 650-0047, Japan, and* [⊥]*RIKEN Center for Developmental Biology, 2-2-3 Minatojima-minamimachi, Chuo-ku, Kobe 650-0047, Japan*

Received April 13, 2010; Revised Manuscript Received May 27, 2010

ABSTRACT: Elucidation of the basis of interactions between biological molecules is essential for the understanding of living systems. Src-homology 3 (SH3) domains play critical roles in interaction networks of proteins by recognizing a proline-rich sequence motif, PxxP. There are, however, several SH3 domains that specifically bind to polypeptide chains without the conventional recognition sequence. The SH3 domain of DDEF1 associates with the SAMP motifs of the adenomatous polyposis coli (APC) tumor suppressor. The SAMP motifs are indispensable for the normal function of APC in tumor suppression. Here we present the structural basis of the interaction between the DDEF1-SH3 domain and the APC-SAMP motifs. We determined the solution structures of the DDEF1-SH3 domain both in a free state and in a complex with APC-SAMP. As the affinity of the interaction was not sufficiently high for the determination of the complex structure in solution by conventional methods, we utilized a fusion protein of the DDEF1-SH3 domain and APC-SAMP. The structures revealed that the SAMP motif adopts a class II polyproline type II helix even though it does not contain the PxxP motif and that a characteristically large hydrophobic pocket of the SH3 domain confers high selectivity to the interaction. Furthermore, investigation into the backbone dynamics of the free and bound systems by NMR spin relaxation experiments demonstrated that the DDEF1-SH3 domain exhibits high flexibility at the peptide recognition site in the absence of the ligand and that most residues of the APC-SAMP motif display extensive local motions even in the stable complex.

Almost all biological processes are maintained through interactions of proteins with their partner ligands. A typical example demonstrating the importance of the associations of proteins with their ligands is signal transduction. Proteins that are involved in signaling pathways are often modular, consisting of several domains and polypeptide motifs, which serve as platforms for interaction with their binding partners. Src-homology 3 (SH3)[1] domains make up one family of such protein modules that are found in many signal transduction proteins (*1*, *2*). Although they do not possess any catalytic functions, they play important roles in mediating molecular interactions.

The structural basis of the interaction between SH3 domains and their associated ligands has been well characterized (*3*, *4*). SH3 domains have a β-barrel structure comprised of five β-strands and have a cleft consisting mainly of hydrophobic residues on their surface. The hydrophobic cleft provides a suitable environment for certain polypeptide sequence motifs to interact with the SH3 domains. A canonical amino acid sequence that associates with SH3 domains is a proline-rich sequence motif, known as PxxP, where x represents any amino acid. The ligand peptides containing the PxxP motif adopt a polyproline type II (PPII) helix when interacting with SH3 domains, and the two proline residues in the polypeptide chain are located over hydrophobic pockets at the cleft of the domains. Because of the pseudo-2-fold symmetry of the PPII helix, the ligands can bind to SH3 domains in two opposite orientations. The direction of the peptides is fundamentally determined by a positively charged residue positioned either to N- or C-terminal end of the PxxP sequence. Depending on the orientation upon the binding to SH3 domains, the ligands are classified as either class I or class II. The consensus sequences of these types of ligand peptides are [+]xΦPxxP and PxΦPx[+], respectively, where Φ represents a hydrophobic residue and [+] a positively charged one.

Several SH3 domains, however, selectively associate with amino acid sequences that lack the PxxP motif. For instance, Gads-SH3 binds to a (R/K)xx(R/K) motif (*5*), and the SH3 domain of Bin1 selects for (K/R)xxxxKx(K/R)(K/R) (*6*). The structure of the (R/K)xx(R/K) motif on the SH3 domain uncovered a unique conformation characterized by an extended N-terminal region and a right-handed 3_{10} helix at the RxxK locus (*7*). In addition, we determined that the SH3 domain of development- and differentiation-enhancing factor 1 (DDEF1; also known as AMAP1 or ASAP1) interacts with the SAMP motifs of adenomatous

[†]This work was supported in part by a Grant-in-Aid for the Japan Society for the Promotion of Science (JSPS) Fellows (to S.K.).

[‡]The atomic coordinates and structure factors of the DDEF1-SH3 domain and the DDEF1-SH3 domain bound to the APC-SAMP1 motif have been deposited in the Protein Data Bank as entries 2RQT and 2RQU, respectively. The resonance assignments of the free DDEF1-SH3 domain and the DDEF1-SH3−APC-SAMP1 complex have been deposited in the Biological Magnetic Resonance Data Bank as entries 11081 and 11082, respectively.

*To whom correspondence should be addressed. E-mail: tiik@protein.osaka-u.ac.jp. Phone: +81 6 6879 4334. Fax: +81 6 6879 8600.

[1]Abbreviations: 2D, two-dimensional; 3D, three-dimensional; aa, amino acid(s); APC, adenomatous polyposis coli; DDEF1, development- and differentiation-enhancing factor 1; FAK, focal adhesion kinase; HSQC, heteronuclear single-quantum correlation; NMR, nuclear magnetic resonance; NOE, nuclear Overhauser effect; NOESY, nuclear Overhauser effect spectroscopy; PPII, polyproline type II; RGS, regulator of G protein signaling; rmsd, root-mean-square deviation; SH3, Src-homology 3.

Published on Web 05/28/2010

polyposis coli (APC), which contain a characteristic Ser-Ala-Met-Pro sequence (*8*).

Both DDEF1 and APC are implicated in the regulation of the cytoskeleton. DDEF1 is one of the GTPase-activating proteins (GAPs) of the ADP ribosylation factors (ARFs), members of small GTPases, which regulate endocytosis, vesicle trafficking, and cytoskeletal remodeling (*9*). On the other hand, APC was first identified as a tumor suppressor (*10*, *11*) and was also found to be one of the microtubule-associating proteins (*12*, *13*). APC associates with microtubules directly, stabilizes them, and also promotes their net growth. Apart from the regulation of microtubules, several other functions of APC are also known (*14*, *15*). The best-characterized function is the downregulation of the Wnt signaling pathway through the association with Axin1, one of the other components of the signal transduction pathway (*16*). APC interacts with the regulator of the G protein signaling (RGS) domain of Axin1 at the SAMP motifs (*17*). APC has three SAMP motifs, and the presence of at least one of them is essential for the protein to exert its tumor suppressing function (*18*). Since previous studies showed that Wnt signaling is involved in the development of cancer, tumor suppression by APC has been discussed only in connection with the signaling pathway. The identification of the interaction of the SAMP motifs with the DDEF1-SH3 domain, therefore, has shed new light on a correlation between the tumor suppressing function and the regulation of the cytoskeleton (*8*).

In the previous paper, we showed that the SH3 domain of DDEF1 interacts with the SAMP motifs of APC, although it does not contain the canonical PxxP motif, that both proteins colocalize at microtubule ends in *Xenopus* A6 cells, and that DDEF1 and APC cooperatively regulate the distribution of the microtubules and focal adhesions in cells (*8*). To clarify the molecular basis of the interaction between the SH3 domain of DDEF1 and the SAMP motifs of APC, we conducted a structural analysis of their complex. In this paper, we report the solution structures of the SH3 domain of DDEF1 derived from human both in a free form and in a complex state with the first SAMP motif (SAMP1) of human APC. Since the affinity of the interaction between the SH3 domain and the SAMP1 motif was not sufficiently high to determine the high-resolution complex structure in solution, we constructed a fusion protein by connecting the domain and the motif with a flexible linker to enhance their apparent affinity. We also studied the dynamical properties of the DDEF1-SH3 domain in the free form and the DDEF1-SH3−APC-SAMP1 complex by ^{15}N spin relaxation.

MATERIALS AND METHODS

Sample Preparation. Human DDEF1 cDNA and APC cDNA were obtained from OriGene Technologies, Inc. and Dr. Akiyama (The University of Tokyo, Tokyo, Japan), respectively. To generate proteins in *Escherichia coli*, DNA fragments were inserted into the pET32a plasmid (Novagen). The fragments used encode human DDEF1 amino acids (aa) 1057−1129, human APC aa 1561−1596 for isolated SAMP1, human APC aa 1578−1596 for the fusion protein, and a four-residue linker, GGGS, for the fusion protein. The fusion protein of DDEF1-SH3 and APC-SAMP1 was constructed by connecting the C-terminus of the SH3 domain and the N-terminus of the SAMP1 motif with the liker and expressed without the vector-derived N-terminal thioredoxin. Including amino acids derived from restriction sites flanking the sequence that encodes GGGS, the resultant linker in the fusion protein consisted of eight residues. Uniformly ^{15}N-labeled (^{13}C- and ^{15}N-labeled) proteins were expressed by growing *E. coli* cells in an M9 minimal medium supplemented with [$^{12}C_6$]-D-glucose and [$^{12}C_3$]glycerol ([$^{13}C_6$]-D-glucose) and $^{15}NH_4Cl$ as carbon and nitrogen sources, respectively. [15%-^{13}C, U-^{15}N]-labeled proteins were produced by using a medium containing 15% [$^{13}C_6$]-D-glucose, 85% [$^{12}C_6$]-D-glucose, and $^{15}NH_4Cl$. The recombinant proteins were purified as described previously for *Xenopus laevis* DDEF1-SH3 and APC-SAMP1 (*8*). For NMR experiments with free DDEF1-SH3, the protein was dissolved in a 90% H_2O/10% D_2O or 99.9% D_2O buffer containing 20 mM sodium phosphate (pH 7.2), 50 mM NaCl, and 0.02% NaN_3. For titration experiments, 20 mM sodium phosphate (pH 7.4), 150 mM NaCl, 0.02% NaN_3, and 10% D_2O were used as a buffer solution. In experiments with the DDEF1-SH3−APC-SAMP1 complex, a sample solution contained 5 mM sodium phosphate (pH 7.2), 5 mM d_6-dithiothreitol, and 0.02% NaN_3 in 90% H_2O/10% D_2O or 99.9% D_2O buffer.

NMR Spectroscopy. NMR experiments were performed on a Bruker DRX-500, DRX-600, or DRX-800 spectrometer. The spectrometers were equipped with a room-temperature triple-axis gradient triple-resonance probe (DRX-500, -600, and -800) or a cryogenic triple-resonance probe (DRX-800). All NMR data were processed with NMRPipe (*19*) and analyzed with Sparky 3 (T. D. Goddard and D. G. Kneller, University of California, San Francisco).

The assignment of the DDEF1-SH3 domain in a free form was obtained by analysis of 3D HNCACB, CBCA(CO)NH, HNCO, HN(CA)CO, H(CCO)NH, and H(C)CH-TOCSY spectra. The stereospecific assignment of methyl groups for Val and Leu was achieved by the method of Neri et al. (*20*). Distance restraints for the structure calculation were collected from 3D ^{15}N-edited and broadband ^{13}C-edited NOESY spectra with a mixing time of 100 ms. For the determination of the structure of the DDEF1-SH3−APC-SAMP1 complex, a suite of 3D HNCA, HNCACB, CBCA(CO)NH, HBHA(CBCACO)NH, MQ-(H)CCH-TOCSY (*21*), H(C)CH-TOCSY, ^{15}N-edited NOESY, and aliphatic and aromatic ^{13}C-edited NOESY spectra was recorded to assign resonances. The methyl groups of Val and Leu were assigned stereospecifically as was done for free DDEF1-SH3. Distance restraints were obtained from 3D ^{15}N-edited, aliphatic ^{13}C-edited, and aromatic ^{13}C-edited NOESY spectra with a mixing time of 150 or 300 ms.

NMR titration experiments were performed by recording a sequence of 2D ^{1}H−^{15}N HSQC spectra of [U-^{15}N]DDEF1-SH3 with varying amounts of the nonlabeled APC-SAMP1 peptide. The values of normalized chemical shift perturbations were calculated as $[\Delta\delta_H^2 + (0.14\Delta\delta_N)^2]^{1/2}$, where $\Delta\delta_H$ and $\Delta\delta_N$ are the changes in the chemical shifts of ^{1}H and ^{15}N, respectively. The equilibrium dissociation constant was extracted by globally fitting a model equation to every titration curve available by nonlinear least-squares minimization.

Backbone ^{15}N R_1, ^{15}N R_2, and ^{15}N−{^{1}H} heteronuclear NOE experiments were conducted at 5 °C and 14.1 T. All experiments were conducted in an interleaved manner. Relaxation delays were as follows: 5, 305 (twice), 605, 905, 1205, 1505, 2005, and 2505 ms for the R_1 experiments with both DDEF1-SH3 and the DDEF1-SH3−APC-SAMP1 complex; 7, 28 (twice), 50, 72, 93, 122, 151, and 180 ms for the R_2 experiment with DDEF1-SH3; and 7, 28 (twice), 50, 72, 93, 115, 136, and 158 ms for the R_2 experiment with the DDEF1-SH3−APC-SAMP1 complex. In the ^{15}N−{^{1}H} heteronuclear NOE experiments, data sets were collected in the

presence and absence of 5 s ^{1}H on-resonance irradiation with a 6 s interscan delay.

Structure Calculation and Refinement. All NOE peaks were picked and assigned manually. Every NOE-derived intraresidual distance restraint was removed in the structure calculation. Dihedral angle restraints for the backbone Φ and Ψ angles were derived from TALOS (*22*) using the chemical shifts of $^{1}H^{\alpha}$, $^{13}C^{\alpha}$, $^{13}C^{\beta}$, $^{13}C'$, and ^{15}N nuclei. The 100 initial structures were calculated using CYANA2.1 (*23*), and the 50 structures with the lowest target function values were subsequently refined in explicit water employing Aria2 (*24*). The 20 lowest-energy structures were selected to form the final ensemble. The structures were analyzed using PROCHECK-NMR (*25*). All molecular graphics images were produced using the UCSF Chimera package (*26*).

Relaxation Data Analysis. R_1 and R_2 values were obtained by fitting the measured peak heights for every relaxation delay time to a single-exponential decay curve using an in-house written program. $^{15}N-\{^{1}H\}$ heteronuclear NOE values were derived from the ratio of the peak intensities with and without ^{1}H saturation. Uncertainties were estimated on the basis of the noise levels in the spectra. The rotational diffusion tensor and the overall rotational correlation time were estimated using Tensor2 (*27*) and r2r1_diffusion (A. G. Palmer, III, Columbia University, New York, NY). The relaxation rates were then analyzed according to the Lipari−Szabo formalism (*28*, *29*) by employing Modelfree4 (*30*, *31*). The chemical shift anisotropy of the ^{15}N nuclei was assumed to be uniform with a value of −160 ppm, and the length of the $^{1}H-^{15}N$ bonds was set to 1.02 Å.

RESULTS

Determination of the Structure of the DDEF1-SH3 Domain. By using high-resolution solution-state NMR spectroscopy, we first determined the three-dimensional (3D) structure of the SH3 domain of human DDEF1 in a free state. The NMR ensemble of 20 structures is shown in Figure 1a. Figure 1b presents a ribbon diagram of the lowest-energy structure in the ensemble. Resonance assignment was accomplished by analysis of a series of triple-resonance NMR spectra. Distance restraints were obtained from ^{13}C- and ^{15}N-edited NOESY spectra. In total, 1024 distance restraints were collected via manual assignment of the NOESY spectra and included in the structure calculation, along with 77 dihedral angle restraints and 25 hydrogen bond restraints, which were predicted from structures generated with the NOE-derived distance restraints and the chemical shift-based dihedral angle restraints. We conducted the structure reconstruction by the simulated annealing torsion angle dynamics and subsequent refinement by the Cartesian dynamics in explicit solvent. For well-defined residues R1071−I1126, the root-mean-square deviations (rmsds) of the backbone N, C^{α}, and C' atoms and all heavy atoms were 0.29 ± 0.05 and 0.75 ± 0.08 Å with respect to the average structure of the ensemble, respectively. The statistics of the structures are summarized in Table 1.

The structure of DDEF1-SH3 takes a β-barrel fold, which is typical of SH3 domains. DDEF1-SH3 consists of one 3_{10} helix (aa 1121−1125) and five β-strands [β1 (aa 1070−1075), β2 (aa 1092−1100), β3 (aa 1103−1110), β4 (aa 1115−1120), and β5 (aa 1125−1127)] that form two β-sheets sharing strand β2. The 3_{10} helix is located between β4 and β5, and between the other strands are loops, namely, the RT loop between β1 and β2, the n-Src loop between β2 and β3, and the distal loop between β3 and β4. Among SH3 domains whose structures have been deposited in the Protein Data Bank (PDB), the third SH3 domain of SH3

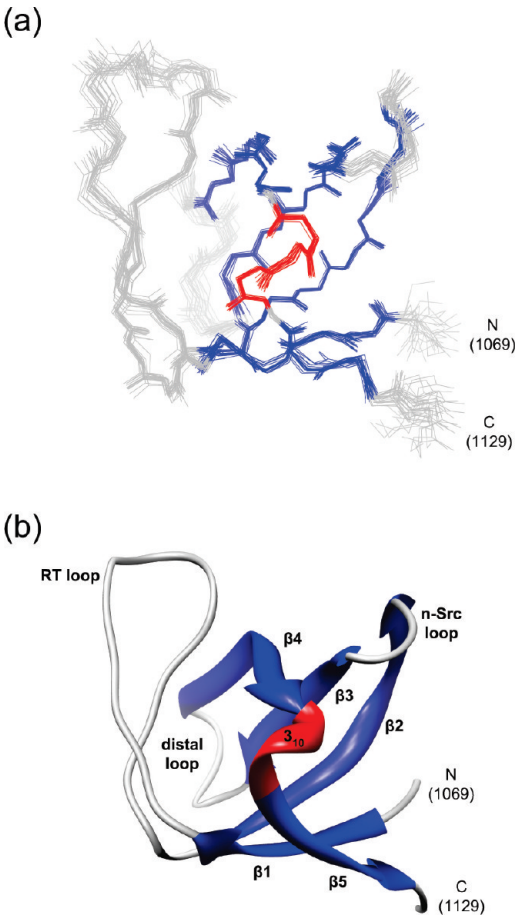

FIGURE 1: 3D structure of the DDEF1-SH3 domain in solution. (a) Ensemble of 20 structures of DDEF1-SH3 as determined in a free state. Residues are colored according to the type of secondary structure: β-sheet, blue; 3_{10} helix, red; otherwise, gray. (b) Ribbon representation of the lowest-energy structure in the ensemble. The color scheme is the same as in panel a.

domain kinase binding protein 1 (PDB entry 2DA9) displayed the highest degree of sequence similarity to the DDEF1-SH3 domain (40% homologous), with an rmsd between their structures of 1.3 Å, which was calculated by using the Dali server (*32*).

Interaction Site for APC-SAMP1 on DDEF1-SH3. To investigate the interaction between the human DDEF1-SH3 domain and the human APC-SAMP motif, we conducted chemical shift perturbation assays by titrating a nonlabeled APC-SAMP1 peptide (Figure 2a,b) into a solution containing the [U-^{15}N]DDEF1-SH3 domain. Overlaid 2D $^{1}H-^{15}N$ heteronuclear single-quantum correlation (HSQC) spectra of the DDEF1-SH3 domain with varying amounts of the APC-SAMP1 peptide are shown in Figure 2c. The experiments were performed at 298 K, and the molecules were dissolved in 20 mM sodium phosphate buffer (pH 7.4) containing 150 mM NaCl. As we reported by using DDEF1 and APC both derived from *X. laevis* (*8*), a set of amide resonances of the human DDEF1-SH3 domain also exhibited significant chemical shift perturbations in the fast- to intermediate-exchange regime in the chemical shift time scale upon addition of the APC-SAMP1 motif. The residues of peaks that moved considerably as the APC-SAMP1 motif was added were mapped on the solution structure of the free DDEF1-SH3 domain (Figure 2d). The chemical shift perturbations were observed particularly for residues in the RT loop, the n-Src loop, β4, and the 3_{10} helix (Figure 2e). The amide resonances of residues

Table 1: Summary of the Structure Calculations for DDEF1-SH3 and the DDEF1-SH3−APC-SAMP1 Complex

	DDEF1-SH3	DDEF1-SH3−APC-SAMP1 complex
no. of restraints		
distance	1049	1319
intramolecular[a]	1024	1133
DDEF1-SH3	1024	1000
APC-SAMP1	−	133
intermolecular[b]	−	160
hydrogen bond	25	26
torsion angle	77	99
DDEF1-SH3	77	79
APC-SAMP1	−	20
no. of violations		
distance restraint violations > 0.3 Å	0	0
dihedral angle restraint violations > 5.0°	0	0
rmsds from the average coordinate		
residue range	1071−1126	1071−1126 and 1579−1592
backbone N, C, and C′ atoms (Å)	0.29 ± 0.05	0.39 ± 0.09
all heavy atoms (Å)	0.75 ± 0.08	0.78 ± 0.10
Ramachandran plot statistics (%)		
residues in most favored region	85.9	82.8
residues in additionally allowed region	14.1	15.2
residues in generously allowed region	0.0	1.0
residues in disallowed region	0.0	1.0

[a]Distance restraints derived from NOEs between ^{1}H nuclei in DDEF1-SH3 or APC-SAMP1. [b]Distance restraints derived from NOEs between DDEF1-SH3 and APC-SAMP1 in the DDEF1-SH3−APC-SAMP1 complex.

in these regions have often exhibited substantial chemical shift perturbations also for other SH3 domains when their ligands containing the conventional SH3 interacting sequence were added, as seen in the titration experiments with the *Xenopus* DDEF1-SH3 domain with a PxxP motif-containing peptide (*8*), indicating that the SAMP motif, which lacks the PxxP sequence, also binds to the canonical interacting surface of the DDEF1-SH3 domain.

To examine the affinity of the DDEF1-SH3 domain for the APC-SAMP1 motif, we determined the equilibrium dissociation constant, K_d, by globally fitting the values of the chemical shift changes to theoretical titration curves by nonlinear least-squares minimization. The fitted curves for representative residues of the DDEF1-SH3 domain are shown in Figure 2f. The calculated K_d value was 23.6 ± 2.0 μM, which fell into the range of relatively weak interactions in terms of structure determination but, physiologically, was in the range of moderately strong and meaningful interactions.

Determination of the Structure of the DDEF1-SH3−APC-SAMP Complex. Since the equilibrium dissociation constant of the DDEF1-SH3 domain for the APC-SAMP1 motif was on the order of tens of micromolar, a sample of a mixture of the isolated protein and peptide was not practically suitable for the observation of a sufficient amount of intermolecular NOEs for the determination of the structure of their complex. Hence, we constructed a fusion protein of DDEF1-SH3 and APC-SAMP1 with a flexible linker consisting mainly of glycine residues between them (Figure 3a). When they were connected, the apparent concentration of the SAMP1 motif at the proximity of the SH3 domain was increased, so that the domain and peptide parts of a single molecule easily formed the complex even at a 1:1 stoichiometry, as shown in Figure 3b. In this figure, a ^{1}H−^{15}N HSQC spectrum of the uniformly ^{15}N-labeled DDEF1-SH3−APC-SAMP1 fusion protein is displayed in black, and the spectra of the ^{15}N-labeled DDEF1-SH3 domain from the titration experiments (under slightly different conditions vs the conditions of those shown in Figure 2c) are colored purple, blue, cyan, green, yellow, orange, and red, with the increased concentrations of the added SAMP1 peptide. Black peaks indicated by asterisks represent residues of the linker and the APC-SAMP1 motif that were not observable in the titration experiments. Peaks in black corresponding to the residues that showed chemical shift changes upon the addition of the SAMP1 peptide were located in positions further than the individual traces of the chemical shift perturbations, indicating the fusion protein was in a bound form with the same structure as the one that would be taken by the complex of the separate proteins. Note that the fragment of the APC-SAMP1 motif we used in the chemical shift perturbation experiments (Figure 2) was longer than what was incorporated in the fusion protein. The APC-SAMP1 motif in the fusion protein, therefore, was sufficient to interact specifically with the DDEF1-SH3 domain. However, we also observed chemical shift changes in some N- and C-terminal residues (R1071−K1073 and H1125−D1129) of the SH3 domain in the fusion protein compared with the peaks from the titration experiments (indicated by filled triangles and hash marks, respectively, in Figure 3b). The alteration in chemical shifts of the N-terminal residues was probably due to degradation of the DDEF1-SH3 domain during sample preparation steps. Indeed, we did not observe the cross-peaks of the 14 N-terminal residues of the SH3 domain in the fusion protein, which appeared in the spectra of the free state, and we also found by mass spectrometry that the fusion protein was subjected to degradation (Figure S1 of the Supporting Information). Meanwhile, since the C-terminus of the DDEF1-SH3 domain was connected to the flexible linker, the C-terminal residues were expected to have different chemical shifts compared to those of the free SH3 domain. Therefore, these lines of evidence supported the idea that the complex formed by the fusion protein was authentic without being distorted by the incorporation of the linker between the DDEF1-SH3 domain and the APC-SAMP1 motif. We also constructed other fusion proteins, including the one in which the order of the DDEF-SH3 domain and the APC-SAMP1 motif was the opposite of that described above and the one that had a longer linker composed of two or three Gly-Gly-Gly-Ser repeats, and investigated them by comparing their NMR spectra. While their ^{1}H−^{15}N HSQC spectra indicated all of them were in a bound form, we found a small number of intersegmental NOEs in those constructs. We, therefore, concluded that the fusion construct shown in Figure 3 is one of the best for detailed structural studies. We even found, in pursuit of an optimal condition for running NMR experiments, that a low temperature (5 °C), a low salt concentration (0 mM), and a neutral pH (7.2 buffered with 5 mM sodium phosphate) were desirable to facilitate the formation of a more stable complex in the fusion protein. All NMR experiments were, therefore, performed under these conditions.

We determined the structure of the complex between the DDEF1-SH3 domain and the APC-SAMP1 motif using the fusion protein described above. Because of the limitation in sensitivity at low temperatures for most triple-resonance experiments employing multiple through-bond magnetization transfer schemes, ^{13}C- and ^{15}N-edited NOESY spectra were mainly utilized for the assignment of side chains. Of all nonlabile proton nuclei in residues R1570−D1129 of DDEF1-SH3 and

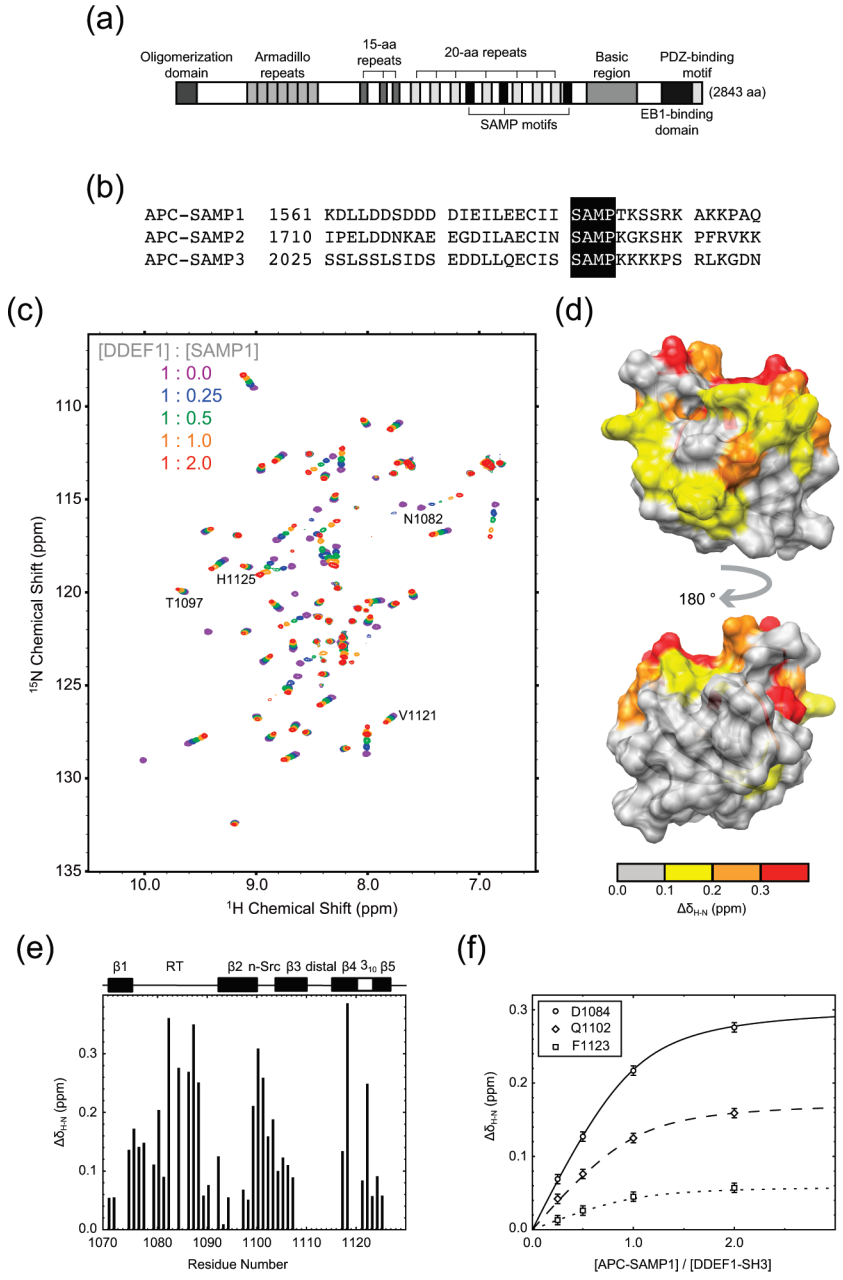

FIGURE 2: Interaction between the DDEF1-SH3 domain and the APC-SAMP1 motif. (a) Domain composition of human APC. (b) Amino acid sequences of the three SAMP motifs of human APC (RefSeq entry NP_001120983). (c) Overlaid $^{1}H-^{15}N$ HSQC spectra of the [U-^{15}N]DDEF1-SH3 domain recorded upon the titration of the nonlabeled APC-SAMP1 motif. Residues that exhibited contributions of R_{ex} to R_2 in the complex form (see Figure 5f) are indicated. (d) Mapping of the residues with the chemical shift changes on the structure of the DDEF1-SH3 domain. Each residue is colored according to the scale of the chemical shift perturbations shown in panel c. The orientation of the SH3 domain at the top is the same as that in Figure 1. (e) Residue-wise chemical shift changes for the DDEF1-SH3 domain caused by the addition of 2.0 equiv of the APC-SAMP1 motif. (f) Titration curves for D1084, Q1102, and F1123 of the DDEF1-SH3 domain. The K_d of the DDEF1-SH3 domain for the APC-SAMP1 motif was estimated to be 23.6 ± 2.0 μM.

C1578−Q1596 of APC-SAMP1, we achieved the assignment of ca. 98%. A total of 1293 distance restraints were also collected from the NOESY spectra, among which 1000 and 133 were between ^{1}H nuclei within DDEF1-SH3 and APC-SAMP1, respectively, and 160 were between protons in the SH3 domain and those in the SAMP1 motif. Ninety-nine dihedral angle restraints and 26 hydrogen bond restraints were also added to the calculation. The structure calculation was conducted in the same manner as that of the free DDEF1-SH3 domain. The ensemble of 20 structures is shown in Figure 4a, whose well-converged residues exhibited rmsds from the average structure of 0.39 ± 0.09 and 0.78 ± 0.10 Å for the backbone N, C^{α}, and C' atoms and for all heavy atoms, respectively. In Figure 4b, a ribbon representation of the lowest-energy structure in the ensemble is presented. The summary of structural statistics is given in Table 1.

Description of the Structure of the DDEF1-SH3−APC-SAMP1 Complex. The structures of the DDEF1-SH3 domain in the free and complex forms did not exhibit any conspicuous conformational changes, except for the rearrangement of the RT loop (Figure S2 of the Supporting Information). The overall secondary structure was almost the same in the two forms. The pairwise rmsd of the structures of the SH3 domain in both ensembles was 0.69 ± 0.13 Å for the backbone N, C^{α}, and C' atoms of

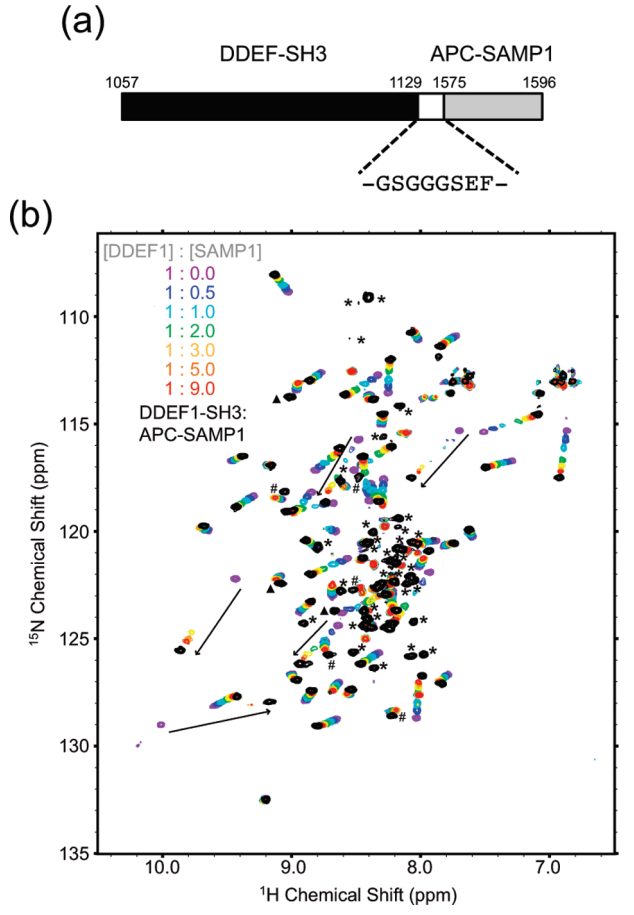

FIGURE 3: Construction of the DDEF1-SH3−APC-SAMP1 fusion protein. (a) Schematic representation of the primary structure of the DDEF1-SH3−APC-SAMP1 fusion protein. (b) $^{1}H-^{15}N$ HSQC spectrum of the [U-^{15}N]DDEF1-SH3−APC-SAMP1 fusion protein (black). The spectrum was superimposed on the overlaid spectra from the titration experiments of the DDEF1-SH3 domain with the APC-SAMP1 motif. Peaks indicated by asterisks were derived from residues in the linker and APC-SAMP1 in the ^{15}N-labeled fusion protein. Filled triangles and hash marks indicate the N- and C-terminal residues, respectively, which showed different chemical shifts compared to those of the free SH3 domain used in the chemical shift perturbation experiments. For peaks that exhibited line broadening in the titration experiments, the chemical shift changes were denoted with arrows for the sake of clarity.

residues from R1071 to I1126, with the largest deviation found for residues A1080−E1085 in the RT loop, whose pairwise rmsd was 1.29 ± 0.45 Å. The arrangement of these residues showed a notable difference when the secondary structural regions of the structures in the two ensembles were superimposed (Figure S1 of the Supporting Information).

The APC-SAMP motif in the bound form adopts a polyproline type II (PPII) helix with its C-terminus oriented toward the specificity pocket (S pocket) of the SH3 domain like the other class II SH3 ligands (Figure 4c). The backbone φ and ψ angles of residues from A1582 to K1586 showed typical values of PPII helices, and the M1583−P1584 pair and the K1586−S1587 pair are located on the two hydrophobic pockets, P1 and P2, respectively, of the SH3 domain situated between aromatic residues, namely Y1076−F1123 and W1104−F1123, respectively. N-Terminal hydrophobic residues, I1579 and I1580, make contact with the DDEF1-SH3 domain at a surface composed of I1075, Y1076, E1090, and H1125. Residues S1587 and S1588 are placed on W1104 of the DDEF1-SH3 domain, a conserved tryptophan residue that is known to disrupt the PPII helices in both the class I and class II peptides, so that the SAMP1 motif is kinked at this position turning into an extended form with a turnlike shape at R1589−K1592, projecting over the S pocket, which is known to be the determinant of the ligand specificity of SH3 domains (*33*). The S pocket of the DDEF1-SH3 domain is surrounded by negatively charged residues, D1084, E1085, E1100, and D1101, while the APC-SAMP1 motif contains a positively charged stretch consisting of R1589, K1590, K1592, and K1593. The abundance of basic residues in the C-terminal part of the APC-SMAP1 motif leads to extensive electrostatic interactions with the acidic residues of the S pocket of the DDEF1-SH3 domain. Although we were not able to obtain direct evidence of salt bridges (direct electrostatic interaction), the collected NOEs and the refined structures suggested potential salt bridges between D1084 and R1589, E1085 and K1592, E1100 and R1589, and D1101 (and/or E1103) and K1590 of the DDEF1-SH3 domain and APC-SAMP1 motif, respectively. We also found that K1586 of the APC-SAMP1 motif, the side chain of which lies along the P2 pocket, can form a salt bridge with D1081 of the DDEF1-SH3 domain. As for the N-terminus (C1578) and the C-terminal residues K1593−Q1596 of APC-SAMP1, we did not identify any NOEs with ^{1}H nuclei of DDEF1-SH3, indicating that a stretch of residues from I1579 to K1592 of the APC-SAMP1 motif associates with the DDEF1-SH3 domain.

Backbone Dynamics of DDEF1-SH3 and APC-SAMP1. Residue-specific ^{15}N longitudinal and transverse relaxation rates (R_1 and R_2) and $^{15}N-\{^{1}H\}$ heteronuclear NOE values of backbone amide ^{15}N spins for the free DDEF1-SH3 domain and the DDEF1-SH3−APC-SAMP1 complex formed by the fusion protein are shown in Figure 5a−c. The experiments were conducted at 278 K on an NMR machine operating at the ^{1}H Larmor frequency of 600.07 MHz. All three relaxation parameters were reliably obtained for 44 and 57 residues for the DDEF1-SH3 domain and the DDEF1-SH3−APC-SAMP1 complex, respectively, and subsequently used for analyses.

To analyze the dynamics of the two systems, we estimated their overall rotational diffusion tensors based on the relaxation rates. The description of molecular tumbling by axial symmetric tensors was justified over isotropic and fully anisotropic representations for both DDEF1-SH3 and the DDEF1-SH3−APC-SAMP1 complex. For the DDEF1-SH3 domain in the free state, the overall rotational correlation time (τ_m) was 15.14 ± 0.19 ns and $D_{\parallel}/D_{\perp}$ was 1.30 ± 0.14, while for the complex, τ_m was 14.17 ± 0.09 ns and $D_{\parallel}/D_{\perp}$ was 1.38 ± 0.07, where $D_{\parallel}$ and $D_{\perp}$ are the parallel and perpendicular components of the principal rotational diffusion tensors, respectively.

The model-free parameters (*28*, *29*) depicting motional properties of the systems were extracted using Modelfree4 (*30*, *31*) and are shown in Figure 5d−f. For the DDEF1-SH3 domain in the free and complex forms, most residues in the secondary structural regions were rigid, with a squared generalized order parameters, S^2, of > 0.9 (Figure 5d). On the other hand, residues comprising the RT loop revealed extensive motional dynamics, exhibiting fast time scale internal motions, the correlation time of which is τ_i, and the contribution of exchange processes, R_{ex}, to the transverse relaxation rates, R_2 (Figure 5e,f). Interestingly, we found that the S^2 values in the RT loop for the complex state of the SH3 domain were increased compared with those in the free form, while τ_i and R_{ex} were decreased, indicating that the motions of the RT loop in the unbound state were weakened in the bound state

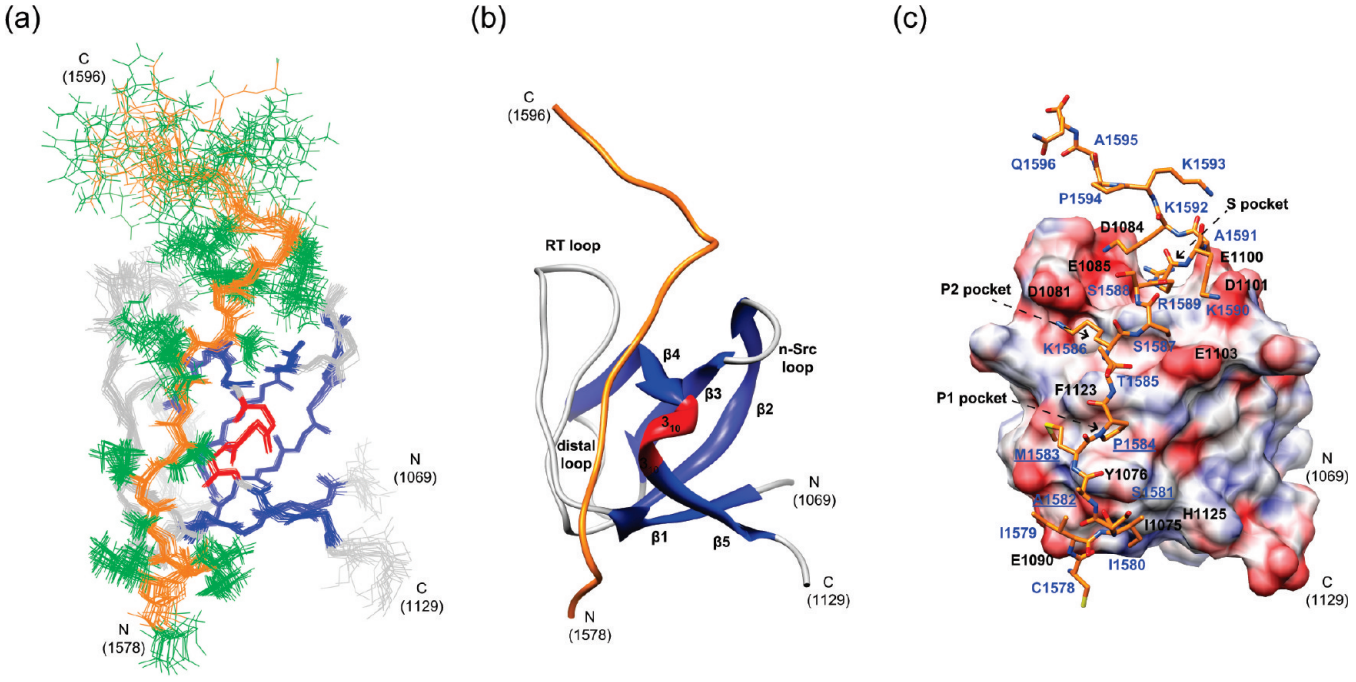

FIGURE 4: Solution structure of the DDEF1-SH3−APC-SAMP1 complex. (a) Ensemble of 20 structures of the DDEF1-SH3−APC-SAMP1 fusion protein. The residues of DDEF1-SH3 are colored according to secondary structure as in Figure 1. The backbone and the side chain atoms of APC-SAMP1 are colored orange and green, respectively. (b) Ribbon diagram of the lowest-energy structure in the ensemble. The color scheme is the same as in panel a. (c) Detailed view of the interaction site. The surface of the DDEF1-SH3 domain is colored on the basis of electrostatic potential (positive, blue; negative, red) calculated by using the PDB2PQR (*39*) and APBS (*40*) programs. The APC-SAMP1 motif is drawn in a stick representation and colored by element. The residues of the DDEF1-SH3 domain and the APC-SAMP1 motif are indicated by black and blue letters, respectively. The underlined residues are the SAMP residues (also in Figures 7 and 8). The nomenclature of the interaction sites of the SH3 domain is based on ref *41* .

(Figure S3 of the Supporting Information). Additionally, there were some residues that exhibited increased R_{ex} values in the complex form relative to the free state (Figure S2c of the Supporting Information). Most of these residues were located at or close to the interaction surface for the APC-SAMP1 motif (e.g., N1082, T1097, V1121, and H1125) and experienced line broadening in the chemical shift perturbation experiments (Figure 2c), suggesting that the extracted R_{ex} values reflect the existence of the association−dissociation exchange.

For the APC-SAMP1 motif in the complex, the obtained model-free parameters were significantly different from those for the DDEF1-SH3 domain in the bound state. All residues but S1587 exhibited large τ_i values of >900 ps (Figure 5e), and little contribution of chemical exchange was present in the backbone of the overall APC-SAMP1 motif (Figure 5f). Intriguingly, the distribution of the generalized order parameters squared for the residues of the APC-SAMP1 motif in close contact with the SH3 domain was not uniform (Figure 5d); the average S^2 for I1579−T1585 was 0.50, while it was 0.77 for S1587−K1592.

DISCUSSION

Structures of the DDEF1-SH3 Domain and the DDEF1-SH3−APC-SAMP1 Complex. In this study, we investigated the structural basis of the interaction between the DDEF1-SH3 domain and the APC-SAMP1 motif, which lacks the conventional SH3 recognition sequence, by determining the 3D structure of the complex as well as that of the free SH3 domain. It is noteworthy that the structure of the DDEF1-SH3−APC-SAMP1 complex was reconstructed by connecting the domain and the ligand in a single polypeptide chain. As the equilibrium dissociation constant of the DDEF1-SH3 domain for the APC-SAMP1 motif showed that the system is dictated by relatively weak interaction in terms of structure determination by NMR, this work demonstrated that the utilization of a fusion protein is a quite robust method for determining the structure of a biomolecular complex.

The ensemble of the calculated structures of the DDEF1-SH3 domain in the free form was well-converged, revealing a typical SH3 fold, although there was an evident feature of note. The DDEF1-SH3 domain lacks an aromatic residue that is conserved among other SH3 domains and has a cysteine, C1078, at that position instead (Figure 6a). The absence of the aromatic ring confers a significant characteristic on the surface structure of the SH3 domain. Compared with other SH3 domains, the P2 pocket of the DDEF1-SH3 domain is particularly large and reaches closer to the RT loop, providing adequate space to accommodate a ligand containing a large or long side chain at an appropriate position (Figure 6b−d). In the DDEF1-SH3−APC-SAMP1 complex, the P2 pocket is occupied by K1586 and S1587 of SAMP1. Our previous study showed that all three SAMP motifs in *X. laevis* APC interact with the DDEF1-SH3 domain of *X. laevis* (*8*). The sequence alignment of the three SAMP motifs of human APC showed that at least one of the residues that could occupy the large P2 pocket is a lysine residue (Figure 2b). This observation provides a clue about the determinant of the specificity and selectivity of the DDEF1-SH3 domain for the APC-SAMP motifs.

The complex structure of the DDEF1-SH3 domain and the APC-SAMP1 motif showed that the ligand interacts with the SH3 domain on the conventional recognition site, a cleft between the RT and n-Src loops, consistent with the results of the NMR titration experiments. The residues from M1583 to K1586 of

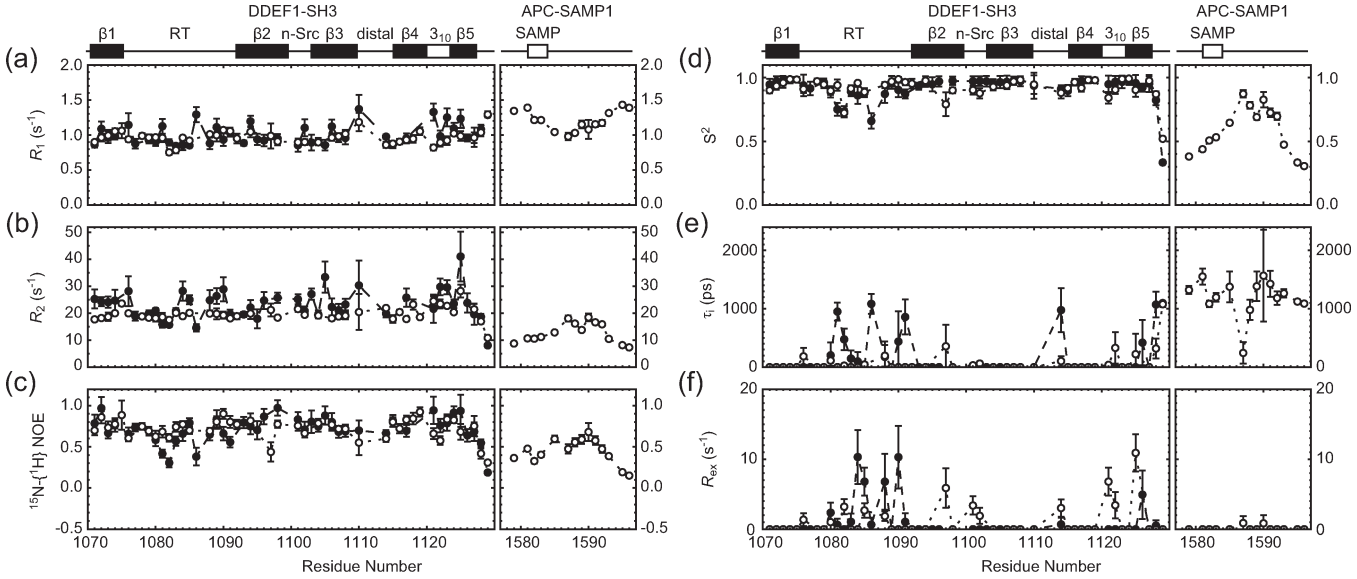

FIGURE 5: Backbone relaxation rates and model-free parameters for DDEF1-SH3 and the DDEF1-SH3−APC-SAMP1 complex. ^{15}N R_1 (a), ^{15}N R_2 (b), and $^{15}N-\{^1H\}$ NOE (c) values of backbone amide ^{15}N spins are plotted vs residue number. Filled and empty circles represent the values for DDEF1-SH3 and the DDEF1-SH3−APC-SAMP1 complex, respectively. (d−f) The model-free parameters, S^2 (d), τ_i (e), and R_{ex} (f), for DDEF1-SH3 (●) and the DDEF1-SH3−APC-SAMP1 complex (○).

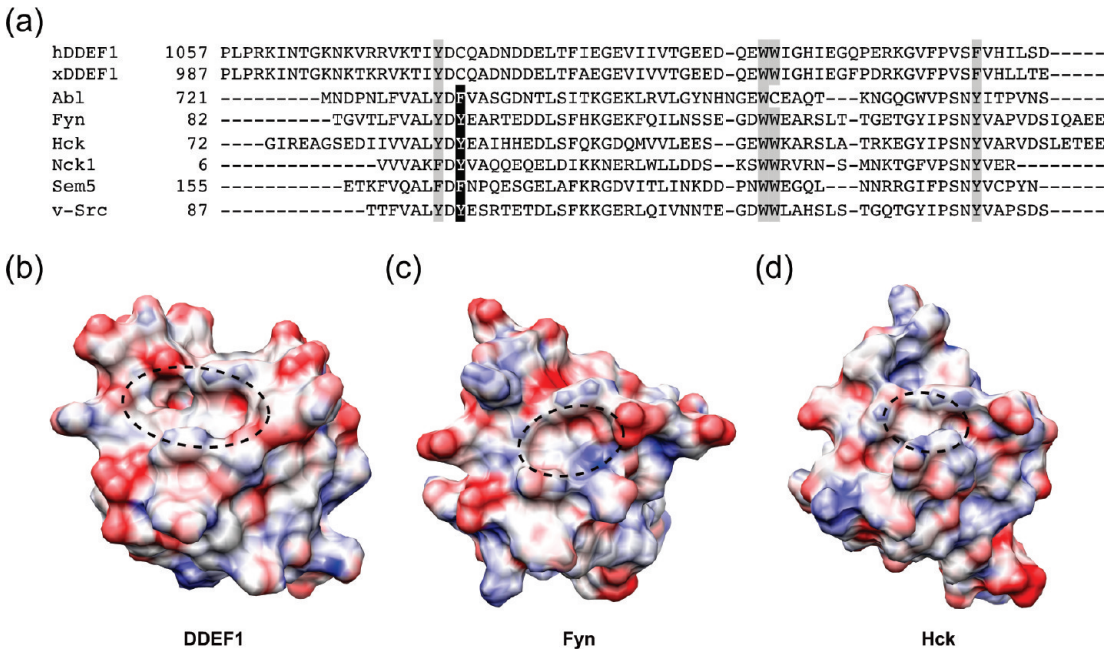

FIGURE 6: Comparison of the structures of SH3 domains. (a) Sequence alignment of SH3 domains. Conserved aromatic residues are displayed with shaded letters. White letters on a black background indicate the position of a conserved aromatic residue that is replaced with cysteine in DDEF1-SH3. (b−d) Structures of DDEF1-SH3 (b), Fyn-SH3 (c) [PDB entry 1NYF (*38*)], and Hck-SH3 (d) [PDB entry 5HCK (*42*)] are shown in a surface representation. The color of each structure is based on electrostatic potential calculated using PDB2PQE (*39*) and APBS (*40*) (positive, blue; negative, red). Dashed circles indicate the P2 pocket of each SH3 domain.

SAMP1 adopt a class II PPII helical conformation (Figure 7a). A difference between the SAMP1 motif and the usual class II ligands in the manner of interaction with their associating SH3 domains is the dipeptide resting on the P2 pocket is Lys-Ser in the former but a two-hydrophobic-residue pair Φ-Pro in the latter (Φ indicates a hydrophobic residue) as in the consensus sequence PxΦPx[+] (*3*, *4*). The lysine residue would be favorable in the case of the DDEF1-SH3 domain, considering the presence of acidic residues adjacent to the P2 pocket as well as the size of the pocket as discussed above. Indeed, we found a potential direct electrostatic interaction between K1586 of SAMP1 and D1081 of DDEF1-SH3, which can stabilize the complex (Figure 4c). The other contact sites in the DDEF1-SH3−APC-SAMP1 complex were similar to those seen in the class II complexes. The M1583-P1584 dipeptide positions itself on the P1 pocket, and furthermore, considerable electrostatic interactions are established between the positively charged residues of the SAMP1 motif and the negatively charged residues in the S pocket of the SH3 domain. The backbone of the SAMP1 motif adopts a turnlike conformation on the S pocket, thereby presumably maximizing the electrostatic interactions between the domain and the ligand. In addition to the canonical interaction sites of SH3 domains for their associated ligands, we

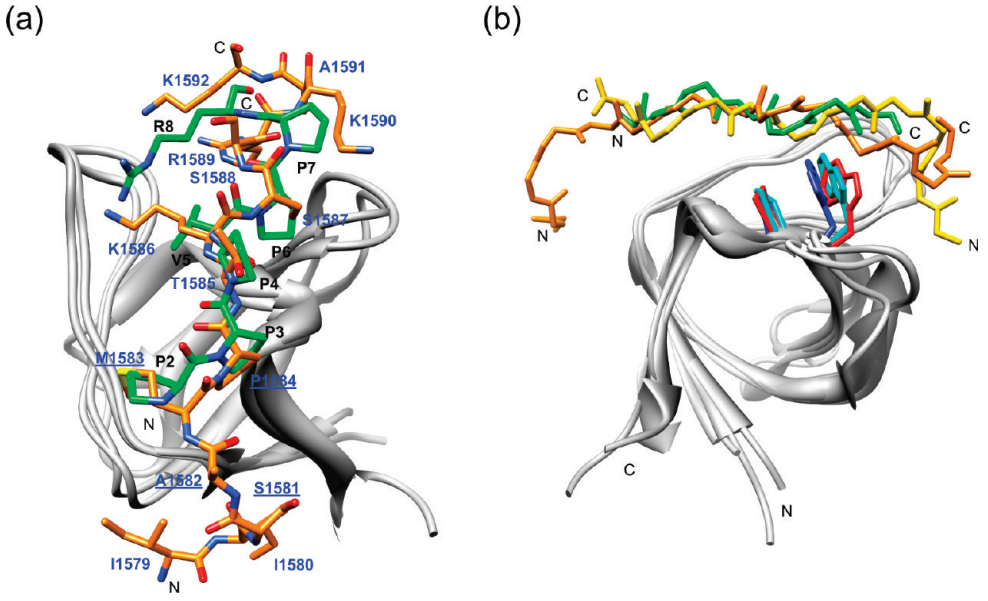

FIGURE 7: Structural comparison of SH3 domain−ligand complexes. (a) Superposition of the 3D structures of the DDEF1-SH3−APC-SAMP1 and class II Sem5-SH3−MSOS [PDB entry 1SEM (*43*)] complexes. The SH3 domains are colored gray, while the ligands are colored by element. The carbon atoms of SAMP1 and MSOS are colored orange and green, respectively. The residues of SAMP1 and MSOS are indicated by blue and black letters, respectively. (b) Superimposed 3D structures of the DDEF1-SH3−APC-SAMP1, class I Abl-SH3−3BP1 [PDB entry 1ABO (*44*)], and class II Sem5-SH3−MSOS complexes. The ligands are colored as follows: orange for APC-SAMP1, gold for 3BP1, and green for MSOS. The SH3 domains are colored gray except for conserved tryptophan and proline residues, which are colored blue, red, and cyan for DDEF1, Abl, and Sem5, respectively, to clarify the tilt angles of the Trp side chains with respect to the Pro residues.

also found a substantial amount of NOEs for residues I1579 and I1580 of the APC-SAMP1 motif with residues I1075, Y1076, and E1090 at the foot of the RT loop of the DDEF1-SH3 domain, suggesting the existence of additional interactions, particularly hydrophobic ones. These lines of evidence support the idea that the association between the APC-SAMP1 motif and the DDEF1-SH3 domain is achieved through a combination of both the conventional and characteristic ways of interactions.

As we showed in the previous study, the SH3 domain of DDEF1 can interact with the APC-SAMP motifs and the site II PxxP motif of focal adhesion kinase (FAK-SII) on the same surface (*8*). We present here the possibility that the SAMP1 motif forms a class II helix when associating with the DDEF1-SH3 domain. This is in agreement with the sequence analysis by Ohba et al. that showed FAK-SII is a class II ligand (*34*). Moreover, as Fernandez-Ballester et al. reported, the selectivity of SH3 domains for the class I or class II ligands depends on the orientation of a conserved tryptophan residue (*35*). Indeed, we found that the tilt angle of the conserved tryptophan W1104 in the DDEF1-SH3 domain corresponds to that observed for the class II SH3 domains rather than for the class I domains (Figure 7b). These findings indicate that the DDEF1-SH3 domain can be classified as a class II SH3 domain and that the APC-SAMP motifs are class II ligands, even though they lack the conventional PxxP sequence.

It is also worth mentioning that the residues of the SAMP motifs involved in the associations with the DDEF1-SH3 domain and the RGS domain of Axin1 are different. The comparison of the structures of DDEF1-SH3−APC-SAMP1 and Axin1-RGS−APC-SAMP3 complexes (*36*) disclosed that residues that are C- and N-terminal to the SAMP sequence are involved in the intermolecular interactions with the DDEF1-SH3 and Axin1-RGS domains, respectively (Figure 8). Some residues, such as the SAMP residues, however, are engaged in the formation of both complexes, indicating that one SAMP motif interacts with only one of the binding partners at a time, which supports our previous results for the binding competition assays (*8*).

Flexibility of the DDEF1-SH3 Domain and the DDEF1-SH3−APC-SAMP1 Complex. The dynamics as well as the structures of proteins play important roles in intermolecular interactions. The results of the backbone ^{15}N spin relaxation experiments and the subsequent model-free analyses illustrated remarkable differences in the dynamic properties between the free and bound states of the DDEF1-SH3 domain. Compared with the SH3 domain in the complex form, the unbound form revealed the existence of extensive local motions in the RT loop. The flexibility in the loop region is decreased when the ligand interacts with the domain. These results suggest that the mobility in the RT loop for the free DDEF1-SH3 domain enables it to effectively capture its specific binding partners. This plasticity may be required for the SH3 domain to accommodate each of the three SAMP motifs as well as the FAK-SII motif, all of which have different amino acid sequences. Since the RT loop of every SH3 domain is long, it is reasonable to assume that it is highly flexible in most SH3 domains. Therefore, a detailed description of the dynamic nature of the loop, including direction and amplitude, would be necessary to fully understand what kind of motion confers specificity to each SH3 domain−ligand interaction.

The relaxation analysis for free DDEF1-SH3 exhibited the presence of chemical exchange for some residues, D1084, E1085, F1088, and E1090, which are located at or close to the binding surface for the APC-SAMP1 motif. We also found that the NMR signals of the SH3 domain in the free state recorded at 278 K are broader than those of the complex with APC-SAMP1. We observed further broadening of the line widths for the free SH3 domain in the absence of NaCl in a buffer solution (data not shown). These results imply the presence of nonspecific associations, especially via electrostatic interactions, between the SH3 domain molecules at the binding site for its ligands. Although the four residues mentioned above did not show significant chemical

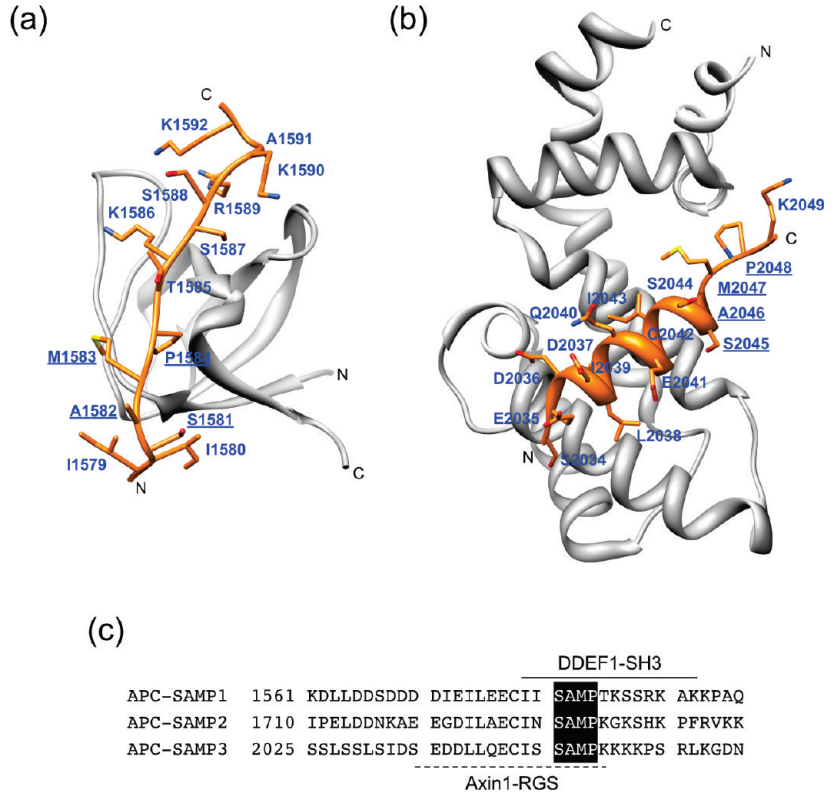

FIGURE 8: Comparison of the structures of the APC-SAMP motif in bound states. (a) Structure of the DDEF1-SH3−APC-SAMP1 complex. The backbone of the APC-SAMP1 motif is shown in a ribbon diagram with the side chains as sticks. The DDEF1-SH3 domain is colored gray. (b) Structure of the Axin1-RGS−APC-SAMP3 complex (PDB entry 1EMU). The SAMP motif is displayed in the same fashion as in panel a. The Axin1-RGS domain is colored gray. (c) Amino acid sequences of the SAMP motifs of human APC. The solid and dashed lines indicate the residues that are involved in the interactions with the DDEF1-SH3 and Axin1-RGS domains, respectively.

shift changes or line broadening upon the addition of the APC-SAMP1 peptide, these observations may reflect the ability of the domain to mediate molecular interactions in this area.

Because the ligands in fusion constructs are isotopically labeled together with the proteins to which they bind, relaxation analyses of the ligands, which have not been performed as frequently as those of its binding partners, can be conducted. Although there is a room for consideration for the difference in the dynamics of the ligands in fusion constructs compared with the isolated ligands, studies of ligand dynamics will still provide further insight into the dynamics of biomolecules. We found that the APC-SAMP1 motif in the complex state is more flexible than the SH3 domain. The C-terminal part of the motif was rigid compared with N-terminal residues. The C-terminal residues of the APC-SAMP1 motif place themselves on the S pocket of the SH3 domain. It is widely accepted that interactions at the S pocket determine the specificity of SH3 domains for their ligands (*33*). The restricted motions of the backbone for the residues of the ligand located on the S pocket may be the result of a particular arrangement necessary for the specific interaction. On the other hand, it is noteworthy that the number of NOEs for the APC-SAMP1 motif with the DDEF1-SH3 domain is small at the C-terminal region compared with the N-terminal part. As basic residues are abundant in the C-terminal part whereas the N-terminal residues are mainly hydrophobic ones, these observations may reflect the motions of their side chains rather than the backbone: the side chains of the hydrophobic residues would need to be stiffer than those of the charged residues to interact correctly with the binding partner. We also found that large backbone local motions were present in the APC-SAMP1 motif. Similar results were observed for the intramolecular complex of the SH3 domain with the proline-rich peptide (Pr) segment in the diphtheria toxin repressor (*37*). The study by Bhattacharya et al. (*37*) demonstrated that the Pr segment undergoes rapid fluctuations on the 0.6−1.0 ns time scale in the bound state. An analogous conclusion could be drawn for the APC-SAMP1 motif in the complex form. The fact that almost all the residues in the APC-SAMP1 motif exhibited extensive dynamics suggests that the ligand has a relatively large conformational space even when it forms the stable complex with the SH3 domain.

ACKNOWLEDGMENT

We thank Dr. Tetsu Akiyama (The University of Tokyo) for providing us with the cDNA of human APC.

SUPPORTING INFORMATION AVAILABLE

Figures of the mass analysis of the DDEF1-SH3−APC-SAMP1 fusion protein, structural comparison of the DDEF1-SH3 domain in the free and complex forms, and differences in the model-free parameters for the DDEF1-SH3 domain in the two states. This material is available free of charge via the Internet at http://pubs.acs.org.

REFERENCES

1. Birge, R. B., Knudsen, B. A., Besser, D., and Hanafusa, H. (1996) SH2 and SH3-containing adaptor proteins: Redundant or independent mediators of intracellular signal transduction. *Genes Cells 1*, 595–613.
2. Mayer, B. J. (2001) SH3 domains: Complexity in moderation. *J. Cell Sci. 114*, 1253–1263.

3. Kay, B. K., Williamson, M. P., and Sudol, M. (2000) The importance of being proline: The interaction of proline-rich motifs in signaling proteins with their cognate domains. *FASEB J. 14*, 231–241.
4. Mayer, B. J., and Eck, M. J. (1995) SH3 domains. Minding your p's and q's. *Curr. Biol. 5*, 364–367.
5. Berry, D. M., Nash, P., Liu, S. K.-W., Pawson, T., and McGlade, C. J. (2002) A high-affinity Arg-X-X-Lys SH3 binding motif confers specificity for the interaction between Gads and SLP-76 in T cell signaling. *Curr. Biol. 12*, 1336–1341.
6. Kojima, C., Hashimoto, A., Yabuta, I., Hirose, M., Hashimoto, S., Kanaho, Y., Sumimoto, H., Ikegami, T., and Sabe, H. (2004) Regulation of Bin1 SH3 domain binding by phosphoinositides. *EMBO J. 23*, 4413–4422.
7. Liu, Q., Berry, D., Nash, P., Pawson, T., McGlade, C. J., and Li, S. S.-C. (2003) Structural basis for specific binding of the Gads SH3 domain to an RxxK motif-containing SLP-76 peptide: A novel mode of peptide recognition. *Mol. Cell 11*, 471–481.
8. Matsui, C., Kaieda, S., Ikegami, T., and Mimori-Kiyosue, Y. (2008) Identification of a link between the SAMP repeats of adenomatous polyposis coli tumor suppressor and the Src homology 3 domain of DDEF. *J. Biol. Chem. 283*, 33006–33020.
9. Sabe, H., Onodera, Y., Mazaki, Y., and Hashimoto, S. (2006) ArfGAP family proteins in cell adhesion, migration and tumor invasion. *Curr. Opin. Cell Biol. 18*, 558–564.
10. Groden, J., Thliveris, A., Samowitz, W., Carlson, M., Gelbert, L., Albertsen, H., Joslyn, G., Stevens, J., Spirio, L., and Robertson, M. (1991) Identification and characterization of the familial adenomatous polyposis coli gene. *Cell 66*, 589–600.
11. Kinzler, K. W., Nilbert, M. C., Vogelstein, B., Bryan, T. M., Levy, D. B., Smith, K. J., Preisinger, A. C., Hamilton, S. R., Hedge, P., and Markham, A. (1991) Identification of a gene located at chromosome 5q21 that is mutated in colorectal cancers. *Science 251*, 1366–1370.
12. Mimori-Kiyosue, Y., and Tsukita, S. (2003) "Search-and-capture" of microtubules through plus-end-binding proteins (+TIPs). *J. Biochem. 134*, 321–326.
13. Schuyler, S. C., and Pellman, D. (2001) Microtubule "plus-end-tracking proteins": The end is just the beginning. *Cell 105*, 421–424.
14. Hanson, C. A., and Miller, J. R. (2005) Non-traditional roles for the Adenomatous Polyposis Coli (APC) tumor suppressor protein. *Gene 361*, 1–12.
15. Mimori-Kiyosue, Y., and Tsukita, S. (2001) Where is APC going? *J. Cell Biol. 154*, 1105–1109.
16. Behrens, J., Jerchow, B. A., Würtele, M., Grimm, J., Asbrand, C., Wirtz, R., Kühl, M., Wedlich, D., and Birchmeier, W. (1998) Functional interaction of an axin homolog, conductin, with β-catenin, APC, and GSK3β. *Science 280*, 596–599.
17. Kishida, S., Yamamoto, H., Ikeda, S., Kishida, M., Sakamoto, I., Koyama, S., and Kikuchi, A. (1998) Axin, a negative regulator of the Wnt signaling pathway, directly interacts with adenomatous polyposis coli and regulates the stabilization of β-catenin. *J. Biol. Chem. 273*, 10823–10826.
18. Smits, R., Kielman, M. F., Breukel, C., Zurcher, C., Neufeld, K., Jagmohan-Changur, S., Hofland, N., van Dijk, J., White, R., Edelmann, W., Kucherlapati, R., Khan, P. M., and Fodde, R. (1999) Apc1638T: A mouse model delineating critical domains of the adenomatous polyposis coli protein involved in tumorigenesis and development. *Genes Dev. 13*, 1309–1321.
19. Delaglio, F., Grzesiek, S., Vuister, G. W., Zhu, G., Pfeifer, J., and Bax, A. (1995) NMRPipe: A multidimensional spectral processing system based on UNIX pipes. *J. Biomol. NMR 6*, 277–293.
20. Neri, D., Szyperski, T., Otting, G., Senn, H., and Wüthrich, K. (1989) Stereospecific nuclear magnetic resonance assignments of the methyl groups of valine and leucine in the DNA-binding domain of the 434 repressor by biosynthetically directed fractional ^{13}C labeling. *Biochemistry 28*, 7510–7516.
21. Zheng, Y., Giovannelli, J. L., Ho, N. T., Ho, C., and Yang, D. (2004) Side-chain assignments of methyl-containing residues in a uniformly ^{13}C-labeled hemoglobin in the carbonmonoxy form. *J. Biomol. NMR 30*, 423–429.
22. Cornilescu, G., Delaglio, F., and Bax, A. (1999) Protein backbone angle restraints from searching a database for chemical shift and sequence homology. *J. Biomol. NMR 13*, 289–302.
23. Güntert, P. (2003) Automated NMR protein structure calculation. *Prog. NMR Spectrosc. 43*, 105–125.
24. Rieping, W., Habeck, M., Bardiaux, B., Aymeric Bernard, A., Malliavin, T. E., and Nilges, M. (2007) ARIA2: Automated NOE assignment and data integration in NMR structure calculation. *Bioinformatics 23*, 381–382.
25. Laskowski, R. A., Rullmannn, J. A., MacArthur, M. W., Kaptei, R., and Thornton, J. M. (1996) AQUA and PROCHECK-NMR: Programs for checking the quality of protein structures solved by NMR. *J. Biomol. NMR 8*, 477–486.
26. Pettersen, E. F., Goddard, T. D., Huang, C. C., Couch, G. S., Greenblatt, D. M., Meng, E. C., and Ferrin, T. E. (2004) UCSF Chimera: A visualization system for exploratory research and analysis. *J. Comput. Chem. 25*, 1605–1612.
27. Dosset, P., Hus, J. C., Blackledge, M., and Marion, D. (2000) Efficient analysis of macromolecular rotational diffusion from heteronuclear relaxation data. *J. Biomol. NMR 16*, 23–28.
28. Lipari, G., and Szabo, A. (1982) Model-Free Approach to the Interpretation of Nuclear Magnetic Resonance Relaxation in Macromolecules. 1. Theory and Range of Validity. *J. Am. Chem. Soc. 104*, 4546–4559.
29. Lipari, G., and Szabo, A. (1982) Model-Free Approach to the Interpretation of Nuclear Magnetic Resonance Relaxation in Macromolecules. 2. Analysis of Experimental Results. *J. Am. Chem. Soc. 104*, 4559–4570.
30. Mandel, A. M., Akke, M., and Palmer, A. G., III (1995) Backbone dynamics of *Escherichia coli* ribonuclease HI: Correlations with structure and function in an active enzyme. *J. Mol. Biol. 246*, 144–163.
31. Palmer, A. G., III, Rance, M., and Wrigh, P. E. (1991) Intramolecular motions of a zinc finger DNA-binding domain from Xfin characterized by proton-detected natural abundance ^{13}C heteronuclear NMR spectroscopy. *J. Am. Chem. Soc. 113*, 4371–4380.
32. Holm, L., Kääriäinen, S., and Schenkel, P. R. A. (2008) Searching protein structure databases with DaliLite v.3. *Bioinformatics 24*, 2780–2781.
33. Li, S. S.-C. (2005) Specificity and versatility of SH3 and other proline-recognition domains: Structural basis and implications for cellular signal transduction. *Biochem. J. 390*, 641–653.
34. Ohba, T., Ishino, M., Aoto, H., and Sasaki, T. (1998) Interaction of two proline-rich sequences of cell adhesion kinase β with SH3 domains of p130Cas-related proteins and a GTPase-activating protein, Graf. *Biochem. J. 330* (Part 3), 1249–1254.
35. Fernandez-Ballester, G., Blanes-Mira, C., and Serrano, L. (2004) The tryptophan switch: Changing ligand-binding specificity from type I to type II in SH3 domains. *J. Mol. Biol. 335*, 619–629.
36. Spink, K. E., Polakis, P., and Weis, W. I. (2000) Structural basis of the Axin-adenomatous polyposis coli interaction. *EMBO J. 19*, 2270–2279.
37. Bhattacharya, N., Yi, M., Zhou, H.-X., and Logan, T. M. (2007) Backbone dynamics in an intramolecular prolylpeptide-SH3 complex from the diphtheria toxin repressor, DtxR. *J. Mol. Biol. 374*, 977–992.
38. Morton, C. J., Pugh, D. J., Brown, E. L., Kahmann, J. D., Renzoni, D. A., and Campbell, I. D. (1996) Solution structure and peptide binding of the SH3 domain from human Fyn. *Structure 4*, 705–714.
39. Dolinsky, T. J., Czodrowski, P., Li, H., Nielsen, J. E., Jensen, J. H., Klebe, G., and Baker, N. A. (2007) PDB2PQR: Expanding and upgrading automated preparation of biomolecular structures for molecular simulations. *Nucleic Acids Res. 35*, W522–W525.
40. Baker, N. A., Sept, D., Joseph, S., Holst, M. J., and McCammon, J. A. (2001) Electrostatics of nanosystems: Application to microtubules and the ribosome. *Proc. Natl. Acad. Sci. U.S.A. 98*, 10037–10041.
41. Aitio, O., Hellman, M., Kesti, T., Kleino, I., Samuilova, O., Pääkkönen, K., Tossavainen, H., Saksela, K., and Permi, P. (2008) Structural basis of PxxDY motif recognition in SH3 binding. *J. Mol. Biol. 382*, 167–178.
42. Horita, D. A., Baldisseri, D. M., Zhang, W., Altieri, A. S., Smithgall, T. E., Gmeiner, W. H., and Byrd, R. A. (1998) Solution structure of the human Hck SH3 domain and identification of its ligand binding site. *J. Mol. Biol. 278*, 253–265.
43. Lim, W. A., Richards, F. M., and Fox, R. O. (1994) Structural determinants of peptide-binding orientation and of sequence specificity in SH3 domains. *Nature 372*, 375–379.
44. Musacchio, A., Saraste, M., and Wilmanns, M. (1994) High-resolution crystal structures of tyrosine kinase SH3 domains complexed with proline-rich peptides. *Nat. Struct. Biol. 1*, 546–551.